An Experimental Investigation of Fretting Fatigue in Ti-6Al-4V: the Role of Contact Conditions and Microstructure

T.A. VENKATESH, B.P. CONNER, C.S. LEE, A.E. GIANNAKOPOULOS, T.C. LINDLEY, and S. SURESH

A systematic investigation of the fretting fatigue behavior of the titanium alloy Ti-6Al-4V in both the mill-annealed (MA) and the solution-treated and overaged (STOA) conditions was carried out. A sphere-on-flat fretting fatigue device was used that facilitated real-time control and monitoring of all the relevant parameters such as the contact geometry, contact (normal and tangential) loads, and bulk alternating stress. While different sets of experiments were conducted to examine the influence of the bulk stress, the tangential load, and the normal load, respectively, on fretting fatigue response, the effect of microstructure on fretting fatigue was explored with experiments on the acicular, Widmanstätten, and martensitic microstructures as well. In experiments where the contact loads were maintained constant and the bulk stress was varied, fretting reduced the fatigue strength of Ti-6Al-4V. For this case, the "strength reduction factor" was higher for the experiments with higher tangential loads. For cases where the bulk stress and the normal or the tangential loads were maintained constant, lower fretting fatigue lives were obtained at larger tangential loads and at smaller normal loads. Of all the microstructures studied, preliminary results on the martensitic structure suggest an enhanced fretting fatigue resistance, compared to the basic STOA or the MA microstructure. Using the measured maximum static friction coefficient for Ti-6Al-4V, the experimentally observed contact and stick-zone radii were found to exhibit good agreement with analytical predictions. Furthermore, conditions for crack initiation were determined through the application of the recently developed adhesion model for fretting fatigue. The model predictions of weak adhesion and crack initiation were validated with experimental observations of stick-slip behavior and fretting fatigue failures, respectively.

I. INTRODUCTION

FRETTING fatigue refers to the contact between two surfaces, where small, oscillatory sliding displacements, typically in the range of 2 to 50 μm, occur between the surfaces, while one or both of the contacting surfaces could be subjected to fluctuating stresses. In the presence of aggressive environments, considerable oxidation leading to wear and material removal can occur at the fretted surface. In addition to surface damage, repeated fretting of surfaces can cause a drastic reduction (by a factor of 2 or more) in the fatigue endurance limit and orders of magnitude decrease in fatigue life from that seen under pure axial cyclic loading alone.[1–4] Consequently, fretting fatigue has been recognized as a complex multistage, multiaxial, fatigue-fracture phenomenon involving fatigue crack initiation, early (small) crack propagation, and sometimes either crack arrest or continued growth, ultimately leading to catastrophic failure.

From a theoretical/analytical perspective, approaches to predict fretting fatigue cracking can broadly be classified as one of two types: stress based or fracture mechanics based. The stress-based approach typically involves formulation of multiaxial criteria such as those due to Crossland, Findley, Sines, Smith-Watson-Topper, McDiarmid, Papadopoulos, *etc.* (as reviewed in Reference 5) by considering a combination of stresses at a particular/critical location in the contact zone. One of the appealing features of such a "stress at a point" approach is its relative simplicity. However, because it does not incorporate a length scale in the analysis, this approach has its limitations and it does not capture essential features of fretting fatigue damage such as prediction of crack initiation, location of crack initiation, or crack propagation direction, in all fretting situations. For example, in the cases of various fretting contact geometries,[3] cracks have been observed to initiate in the slip zone or the stick-slip boundary, while the stress-based approaches always predict the fretting cracks to initiate at the edge of the contact.

By incorporating an appropriate lengthscale in the analysis for fretting crack initiation and propagation, the fracture mechanics approach addresses a principal limitation of the stress-based approaches. However, most of the fracture mechanics approaches do not provide a framework for identifying/deriving this lengthscale unambiguously and hence the initial crack length has to be assumed *a priori.*

Recently, a new model for fretting fatigue crack initiation has been developed[6] wherein the effects of interfacial adhesion between the contacting bodies were incorporated in the analysis of the mechanics of contact fatigue. By recognizing that adhesion induces square-root singular stress fields in the contact zone, a fracture mechanics methodology was applied to derive a natural lengthscale for the fretting fatigue problem. A comparison of the cyclic variations in local stress intensity factors with the threshold stress intensity factor range for the onset of fatigue crack growth then provided

T.A. VENKATESH, Postdoctoral Associate, B.P. CONNER, Graduate Student, and S. SURESH, R.P. Simmons Professor, and A.E. GIANNAKOPOULOS, Research Scientist, are with the Department of Materials Science and Engineering, Massachusetts Institute of Technology, Cambridge, MA 02139. T.C. LINDLEY, Lecturer, is with the Department of Materials Science and Engineering, Imperial College of Science, Technology and Medicine, London SW7 2BP, United Kingdom. C.S. LEE, formerly Visiting Scientist at the Massachusets Institute of Technology, is Professor at the Pohang University of Science and Technology, South Korea.

Manuscript submitted August 23, 2000.

critical conditions for crack initiation. It was also shown that the location of crack initiation within the contact area and the initial direction of crack growth from the contact surface into the substrate could be quantitatively determined by this approach.

The experimental investigation of fretting fatigue on various materials (metals, ceramics, and polymers), using different methods/contact geometry (with bridge-type, cylindrical, or spherical fretting pads), indicates that the different stages in fretting fatigue depend to varying extent on a number of material, mechanical, and environmental variables; these include the microstructure, geometry, stresses, temperature, frequency, surface modification, residual stresses, surface roughness, *etc.*[1–4] Given the complexity of the phenomenon, there exists a critical need for developing methods to characterize the fretting behavior of materials in a manner that allows for easy control of all the major variables that influence fretting. Hence, a novel fretting fatigue device that allowed for the real-time control and monitoring of all the pertinent variables in a fretting fatigue experiment was developed[7] and validated with experiments on 7075 T6 aluminum alloy.[8]

Several aspects of the fretting fatigue behavior of the titanium alloy Ti-6Al-4V have been investigated, mostly using a flat-on-flat or a cylinder-on-flat geometry (*e.g.*, References 9 and 10) and to a lesser extent on the sphere-on-flat geometry.[11,12]

The objectives of the current work are as follows. Through a systematic experimental study of the sphere-on-flat fretting fatigue of the titanium alloy Ti-6Al-4V, we

(1) characterize the fretting fatigue response of Ti-6Al-4V and its dependence on the various mechanical and geometrical factors such as the contact (normal and tangential) loads, bulk loads, and fretting pad geometry;
(2) investigate the role of microstructure in the fretting fatigue response of Ti-6Al-4V through experiments on Ti-6Al-4V subjected to different heat treatment schedules;
(3) quantify damage such as the fretting scar size, crack initiation locations, crack propagation angles, and their dependence on the experimental conditions;
(4) identify the different regions of fretting fatigue crack growth from initiation through specimen failure and the fraction of life spent in each of those regions; and
(5) assess the results within the context of the new fretting fatigue adhesion model.

This article is arranged in the following sequence. Section II presents details of the materials and microstructures used, experimental methods employed, and conditions investigated in this study. Section III presents fretting fatigue results from experiments where each of the following variables, normal contact load, tangential load, bulk load, and material microstructure, was varied systematically. In Section IV, the observed microstructural details such as the fretting scars, crack initiation locations, and crack propagation angles are discussed by recourse to classical analysis of the fretting contact as well as through the adhesion model of fretting fatigue. Principal conclusions from this study are presented in Section V.

Table I. Ti-6Al-4V Subjected to Various Heat Treatments to Obtain Different Microstructures

Microstructure	Heat Treatment
STOA	1.25 h at 932 °C in air and air cooled to room temperature; followed by 2 h at 704 °C and fan cooled in argon atmosphere to room temperature
MA	2 h at 704 °C followed by air cooling
Martensitic	0.5 h at 1050 °C followed by water quench
Coarse-grained STOA	48 h at 930 °C followed by air cooling; 12 h at 700 °C followed by air cooling
Acicular	0.5 h at 1050 °C followed by air cooling
Widmanstätten	0.5 h at 1050 °C followed by furnace cooling to 700 °C (1 h) and air cooled to room temperature

II. EXPERIMENTS

A. *Material System*

Two variants of Ti-6Al-4V, with nominal compositions of 6.08 pct Al, 4.01 pct V, 0.19 pct Fe, 0.18 pct O, 0.02 pct C, 0.01 pct N, 0.0004 pct H, <0.001 pct Y and the balance Ti, and 6.30 pct Al, 4.17 pct V, 0.19 pct Fe, 0.19 pct O, 0.13 pct N, and the balance Ti (by weight), respectively, in the mill-annealed (MA) and solution-treated and overaged (STOA) conditions, were selected for the fretting fatigue study. Through appropriate heat treatment schedules (Table I), the basic STOA microstructure was modified further to obtain coarse-grained STOA, martensitic, acicular, and lamellar/Widmanstätten microstructures (Figures 1 through 3).

Optical metallography samples, prepared by polishing with SiC paper, 3 μm diamond solution, 0.3 μm alumina solution, and 0.05 μm Mastermet solution and subsequently etched with a reagent consisting of 5 pct HF, 10 pct HNO_2, and 85 pct distilled water, revealed the microstructural details of the different materials, as described subsequently.

The MA material exhibited a duplex microstructure, with elongated primary alpha grains (10 μm in width by 50 to 80 μm in length) along the longitudinal direction and an equiaxed structure, with an average primary alpha grain size about 5 to 10 μm, in the transverse cross section. The basic STOA material displayed a duplex/bimodal microstructure with primary alpha grains (10 to 20 μm) surrounded by a lamellar matrix with a minor elongation of grains in the longitudinal direction, while the coarse STOA material had a primary alpha grain size between 20 and 25 μm. The martensitic material was characterized by a needlelike microstructure. The acicular microstructure consisted of colonies of coarse lamellar grains with an average colony diameter of approximately 300 μm. The Widmanstätten microstructure had lamellae with a width of about 15 to 20 μm.

Fretting fatigue test samples had rectangular gage cross sections (Figure 4) for all six microstructures. The fretting pads with spherical contact surfaces (Figure 4) were machined from the MA material for the fretting tests on the MA material, while they were machined from the basic STOA material for all other fretting tests. The test samples and the fretting pads were polished with 0.3 μm alumina solution. The pertinent mechanical properties of the test samples and pads are listed in Table II.

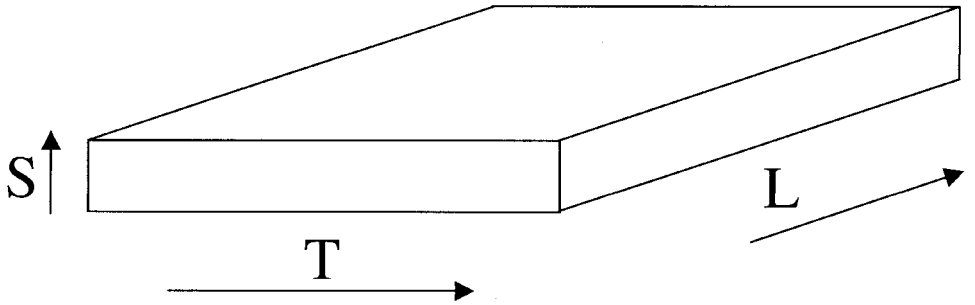

(*a*)

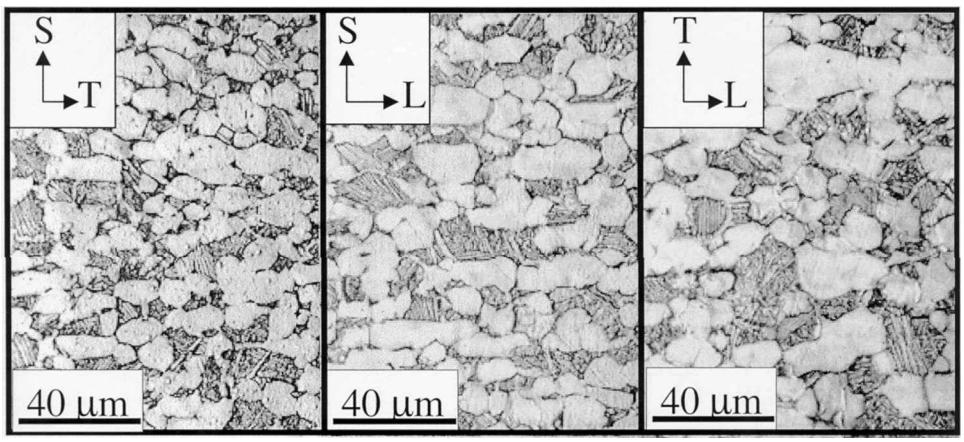

(*b*)

Fig. 1—(*a*) and (*b*) Microstructure of Ti-6Al-4V in the STOA condition. (The various cross sections are illustrated with reference to the as-received ingot (a)).

B. *Fretting Fatigue Experiments*

A fretting fatigue test apparatus (Figure 5) was designed for independent control and accurate, real-time monitoring of all the pertinent experimental variables such as the specimen bulk load, P, the normal, N, and tangential, Q, loads, at the specimen/fretting pad interface, and the relative displacement between the contacting surfaces, δ, as described in more detail in Reference 7.

Briefly, the specimen is subjected to a variable axial load through the actuator of a servohydraulic testing machine, and the normal load is transmitted to the specimen through spring-loaded spherical pads. The supports of the spherical pads are mounted on a compliant system and attached to the structure of the testing machine. Upon the application of the bulk/axial load, P, the resulting strain in the test specimen translates, due to friction at the contact, to a tangential load, $Q = -(C_p/C_q)P$, where C_p and C_q, respectively, are the compliances of the load train and the pad-support system. Experimentally, this tangential load is determined as a sum of the load values measured by the two load cells mounted below the linear bearings. The coupling of Q and P through friction results in the same load ratio, R', between Q and the bulk stress σ_b.

With its many points of adjustment for alignment and compliance, the fretting fatigue device allows for the system compliance to be changed such that the tangential load, or the relative displacement between the specimen and the pads, can be varied systematically while maintaining the normal and bulk loads constant for each test. As discussed in Appendix A, this device also allows for the measurement of the average friction coefficient.

The experimental conditions investigated in this work are summarized in Table III. All tests were conducted in air with 60 to 70 pct relative humidity at 25 °C. The axial load varied from fully tensile to fully compressive (load ratio, $R' = -1$), and the maximum bulk stress never exceeded the endurance limit for this material. The test frequency was 10 Hz. Each side of the specimen was longer than $6a$, where a was the contact radius. Such a constraint on dimensions was necessary to prevent edge effects from interfering with the test.

As the fretting fatigue device allowed for the fretting of two opposite sides of the specimens under identical loading conditions (Figure 5), each fretting test effectively constituted two tests performed under identical conditions. As expected, major fretting fatigue cracks initiated on either of the two contacts.

III. RESULTS

The following sections present results of the fretting fatigue experiments, where the influence of the various factors such as the bulk, normal, and tangential loads, fretting pad geometry, and the material microstructure on fretting damage (*i.e.*, fretting scars and cracks) and total fretting fatigue life was examined systematically.

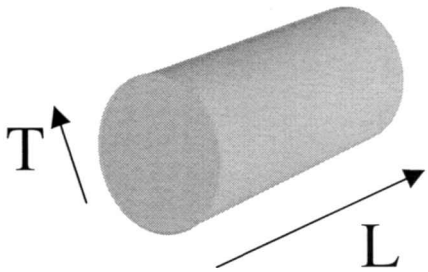

(*a*)

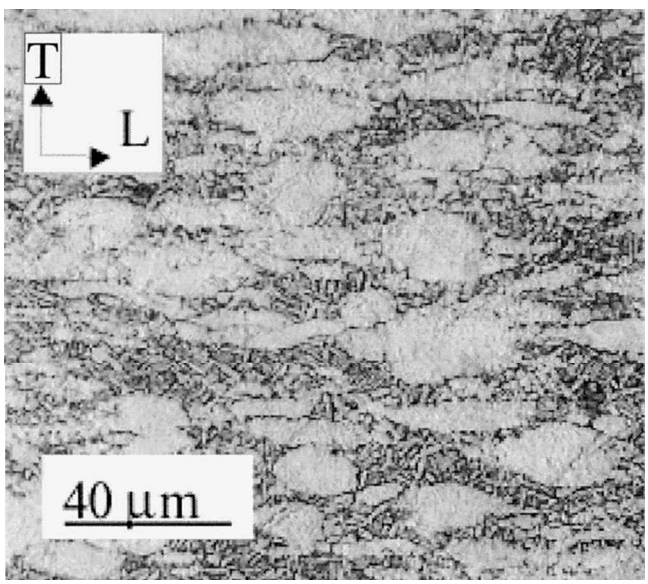

(*b*)

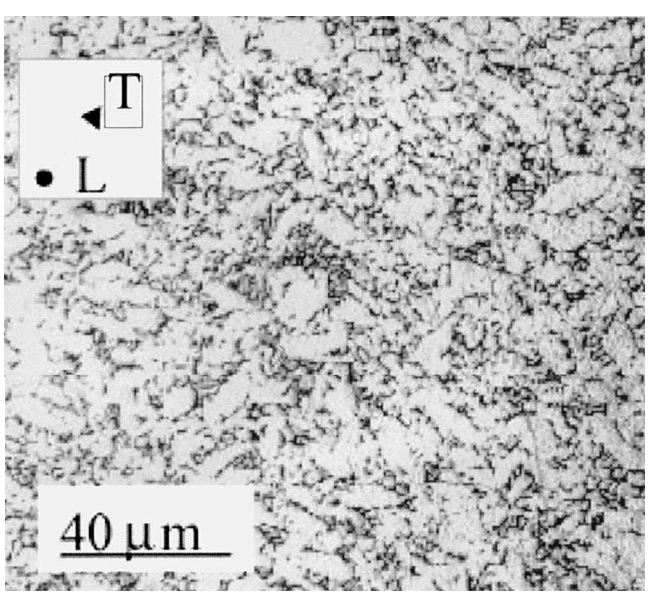

(*c*)

Fig. 2—(*b*) and (*c*) Microstructure of Ti-6Al-4V in the MA condition. (The different cross sections are illustrated with respect to the (*a*) as-received rod).

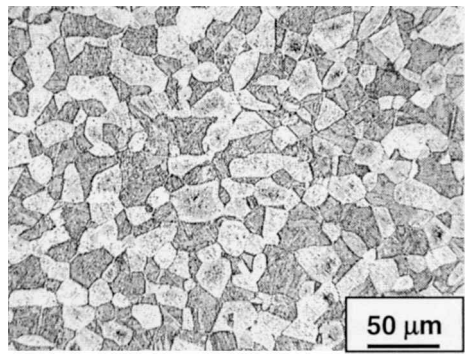

(*a*)

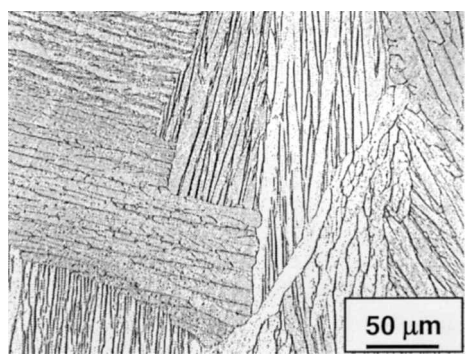

(*b*)

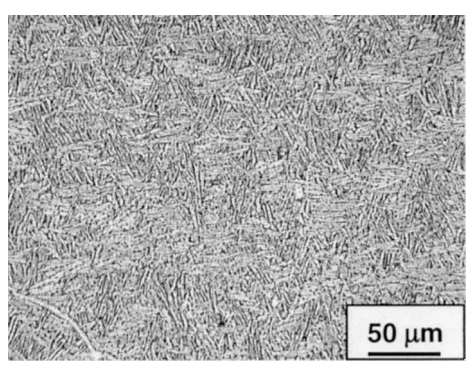

(*c*)

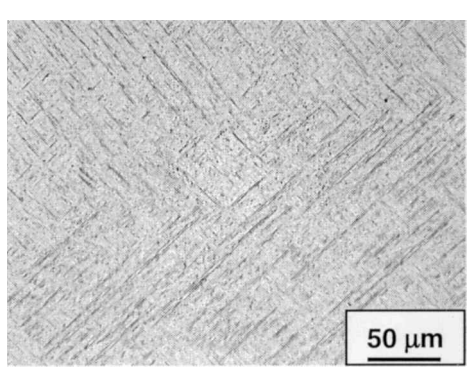

(*d*)

Fig. 3—Various microstructures of Ti-6Al-4V: (*a*) coarse-grained STOA, (*b*) Widmanstätten structure, (*c*) acicular structure, and (*d*) martensitic structure.

A. *Fretting Scars and Cracks*

In all the experiments, the fretted area of the samples displayed scars that were typically characterized by a central stick zone surrounded by an annulus of slip zone, with a slight eccentricity (Figure 6). A significant amount of oxide

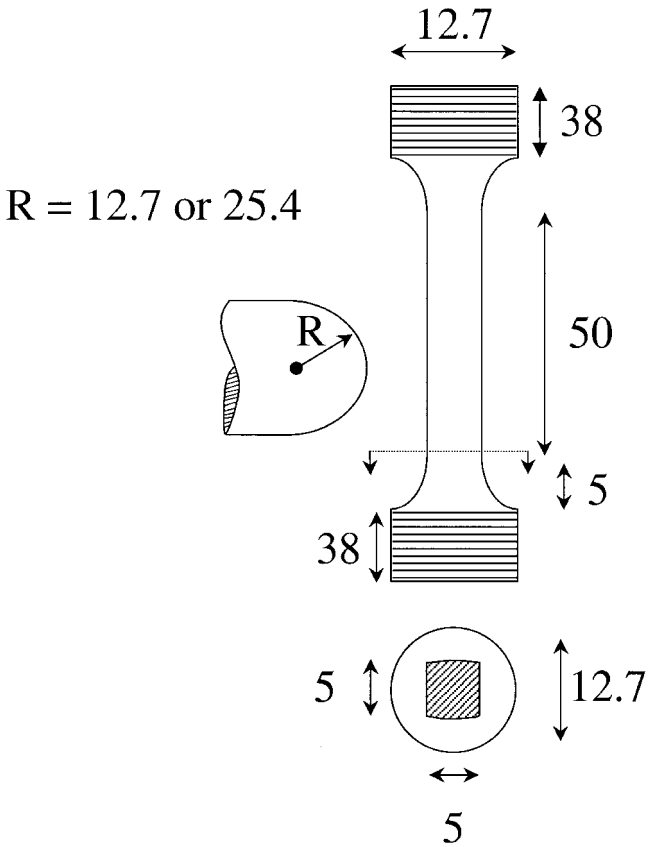

Fig. 4—Schematic of fretting fatigue sample and pad geometry (all dimensions in millimeters, not to scale).

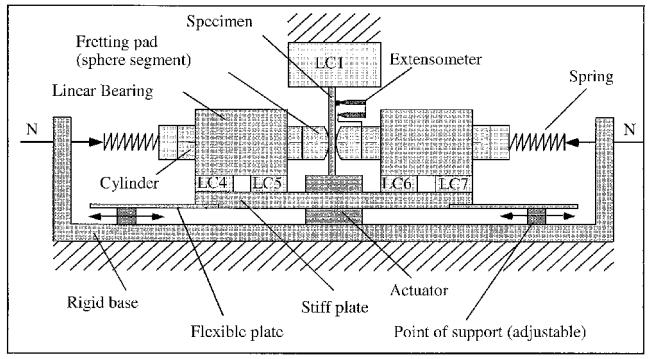

Fig. 5—Fretting fatigue test apparatus.[7] LC = load cell.

debris was also produced by the fretting action at the trailing edge of the contact,* as seen in Figure 6. In each case the scar on the fretting pad was a mirror image of that on the sample surface. Indirect evidence for adhesion between contacting surfaces could be discerned from the fact that some brightly reflecting regions, possibly created by the rupture of microwelds, were also observed in several fretting scars.

*It is believed that gravity in combination with the higher contact stresses present at the trailing edge (Appendix B) may have contributed toward creating this asymmetry in debris accumulation. The effects of this asymmetry on the adhesion debond energies (Section IV) have not been incorporated in the current analysis.

Because the sliding of the samples upon failure typically damaged the scars, the fretting scars were studied in detail in those experiments where sample failure did not occur. The contact zone radius, a, stick-zone radius, c, and the eccentricity, e, observed in the experiments where samples did not fail are presented in Table IV.

Fretting cracks typically initiated near the trailing edge of the contact or in the slip zone close to the trailing edge of the contact (Figure 7, Table III). (For the definition of the trailing edge of the contact, see Appendix B). In some cases, multiple crack initiation sites were also noted.

Upon initiation at the specimen contact surface, the fretting fatigue cracks propagated along the specimen surface in a direction perpendicular to the direction of the bulk load as well as into the interior of the specimen. The crack propagation angle was determined optically by inspecting the fractured surface (details of which are presented in Appendix C).

B. *Effect of the Bulk Stress*

Four sets of experiments (tests 1 through 21, Table III) were performed on the MA material, where for each set, the normal load, the tangential load, and the fretting pad radius were maintained constant while the sample bulk load was varied (Figure 8). In general, the life of the fretted samples increased as the bulk stress decreased with an endurance limit being reached at lower bulk stresses. In all cases, fretting reduced the fatigue strength of Ti-6Al-4V, with the "strength reduction factor" being higher for the experiments with the higher tangential load, $Q = 30$ N, compared to those with the lower tangential load, $Q = 15$ N.

Among all the experiments with a tangential load of 30 N, those experiments with the larger pad radius of 25.4 mm typically exhibited longer lives and a higher fatigue strength. A similar trend was also observed for the experiments with a tangential load of 15 N, where the fatigue for those experiments with the larger pad radius was marginally higher than for the experiments with the lower pad radius.

C. *Effect of the Tangential Load*

Two sets of experiments were performed on the MA (tests 22 through 28, Table III) and STOA material (tests 37 through 46, Table III), where for each set, the normal load,

Table II. The Mechanical Properties of Ti-6Al-4V Used in the Fretting Fatigue Experiments

Properties	MA	STOA	Acicular	Widmanstätten	Martensitic
Elastic Modulus (GPa)	116	116	116	116	116
Poisson's ratio	0.34	0.34	0.34	0.34	0.34
Yield strength (MPa)	963	935	935	855	1137
Tensile strength (MPa)	1016	970	995	890	1243

Table III. List of Experimental Conditions and Results of All the Fretting Fatigue Experiments on Ti-6Al-4V

Experiment	Experimental Input Parameters				N_f	$N_{(III)}$	b_0 (μm)	d_0 (μm)	α (Deg)	Fracture Location	l_c (μm)
	N (N)	Q (N)	σ_b (MPa)	$2R$ (m)							
					Effect of bulk stress (MA Ti-6Al-4V)						
1	50	14.5	394	0.0254	107,899	53,232	280	300	80.7	unclear	283.7
2	50	13	357	0.0254	31,540	—	—	—	—	—	—
3	50	15	341	0.0254	266,176	65,575	180	310	—	eoc	—
4	50	14.5	300	0.0254	474,656	177,275	200	250	—	eoc	—
5	50	15	280	0.0254	2,055,856	147,124	180	310	68.7	eoc	193.2
6	50	15	341	0.0508	192,000	73,473	120	275	—	eoc	—
8	50	15	338	0.0508	1,609,238	84,474	130	255	72.9	oc	136.0
7	50	15	325	0.0508	872,863	104,417	250	300	—	eoc	—
9	50	17	300	0.0508	8,596,572*	—	—	—	—	—	—
10	50	15	292	0.0508	3,962,688	137,493	200	300	—	eoc	—
11	50	15	276	0.0508	4,273,718*	—	—	—	—	—	—
12	50	16	254	0.0508	2,288,839*	—	—	—	—	—	—
13	50	30	315	0.0254	117,183	104,030	150	275	56.3	eoc	180.3
14	50	30	300	0.0254	142,746	132,074	180	280	—	unclear	—
15	50	30	250	0.0254	278,238	247,080	160	210	58.0	eoc	188.7
16	50	33	225	0.0254	691,612	374,035	231	256	68.9	eoc	247.6
17	50	30	375	0.0508	85,957	77,427	180	230	67.4	eoc	194.9
18	50	30	320	0.0508	212,491	179,662	100	170	—	eoc	—
19	50	30	265	0.0508	245,637	178,088	260	350	71.9	eoc	273.5
20	50	30	260	0.0508	253,700	—	150	255	—	eoc	—
21	50	30	225	0.0508	3,295,860	390,790	320	360	73.5	eoc	333.7
					Effect of tangential load (MA Ti-6Al-4V)						
22	50	30	300	0.0254	142,746	132,074	180	280	57.3	unclear	213.9
23	50	23	300	0.0254	307.653	153,745	70	260	75.3	eoc	72.3
24	50	14.5	300	0.0254	474,656	177,275	200	250	75.7	eoc	206.3
25	50	11	300	0.0254	3,057,892	152,907	138	240	82.9	slip zone	138.5
26	50	10	300	0.0254	2,163,277	399,807	360	250	72.8	slip zone	376.8
27	50	32	300	0.0508	207,258	120,466	—	—	—	—	—
28	50	21	300	0.0508	598,191	140,926	150	210	71.6	oc	158.0
					Effect of normal load (MA Ti-6Al-4V)						
29	70	16.5	300	0.0254	2,969,846	144,293	150	250	75.1	slip zone	155.2
30	60	16.3	300	0.0254	1,235,575	147,827	140	250	60.2	slip zone	161.3
31	50	14.5	300	0.0254	474,656	177,275	200	250	75.3	eoc	206.7
32	40	16	300	0.0254	401,153	183,118	90	200	60.9	eoc	103.0
33	30	16	300	0.0254	499,291	258,959	75	150	61.9	eoc	85.0
34	22	15	300	0.0254	284,670	184,700	100	200	—	eoc	—
35	30	17	300	0.0508	5,342,499	199,458	100	250	65.8	eoc	109.6
36	25	17	300	0.0508	12,000,000*	—	—	—	—	—	—
					Effect of tangential load (STOA Ti-6Al-4V)						
37	50	37.5	300	0.0254	182,617	163,544	222	272	65.3	eoc	244.3
38	50	23	300	0.0254	227,972	124,413	222	309	77.2	slip zone	227.6
39	50	21	300	0.0254	317,073	241,400	185	210	70.9	eoc	195.7
40	50	20	300	0.0254	260,894	179,285	160	228	79.0	eoc	162.9
41	50	18	300	0.0254	433,195	281,618	185	198	70.1	slip zone	196.7
42	50	17	300	0.0254	605,023	162,264	197	259	72.0	slip zone	207.1
43	50	14	300	0.0254	745,000	257,406	148	185	78.4	slip zone	151.0
44	50	13	300	0.0254	1,955,612	147,613	123	241	59.3	eoc	143.0
45	50	20.5	300	0.0508	244,054	162,583	173	241	68.3	eoc	186.2
46	50	18.3	300	0.0508	4,708,273	142,253	148	253	55.4	eoc	179.8
					Effect of microstructure						
47	50	30.5	300	0.0254	194,260	—	—	—	—	—	—
48	50	24	300	0.0254	4,720,061*	—	—	—	—	—	—
49	50	24	300	0.0254	227,100	—	—	—	—	—	—

Table III. Continued. List of Experimental Conditions and Results of All the Fretting Fatigue Experiments on Ti-6Al-4V

	Experimental Input Parameters										
Experiment	N (N)	Q (N)	σ_b (MPa)	$2R$ (m)	N_f	$N_{(III)}$	b_0 (μm)	d_0 (μm)	α (Deg)	Fracture Location	l_c (μm)
50	50	20	300	0.0254	369,920	—	—	—	—	—	—
51	50	16	300	0.0254	1,100,649*	—	—	—	—	—	—
52	50	14	300	0.0254	1,501,900*	—	—	—	—	—	—
53	50	20.5	300	0.0254	240,501	—	114	235	52.1	eoc	144.4
54	50	15.5	300	0.0254	378,782	—	102	248	57.9	eoc	120.4
55	50	26	300	0.0254	271,576	—	—	—	—	eoc	—
56	50	19.5	300	0.0254	290,286	—	190	337	—	slip zone	—
57	50	14	300	0.0254	936,000	—	—	—	—	eoc	—

Key: N = normal contact load; Q = tangential contact load; σ_b = maximum bulk stress; $2R$ = diameter of fretting pad; N_f = total number of fatigue cycles to failure; $N_{(III)}$ = number of cycles spent in region III; $N_{(I+II)}$ = number of cycles spent in regions I and II = $[N_f - N_{(III)}]$; b_0 and d_0 = crack geometry at the beginning of region III; α = average angle of crack initiation into the specimen; eoc = edge of contact; oc = outside the contact zone; l_c = length of crack in region II; and * = samples did not fail. Tests 1 through 36 were performed on MA Ti-6Al-4V (with MA fretting pads); tests 37 through 46 were performed on the Ti-6Al-4V in the STOA structure (with STOA fretting pads); tests 47 through 52, 53 through 54, 55 through 56, and 57 corresponded, respectively, to martensitic, coarse STOA, Widmanstätten, and acicular microstructures (with STOA fretting pads).

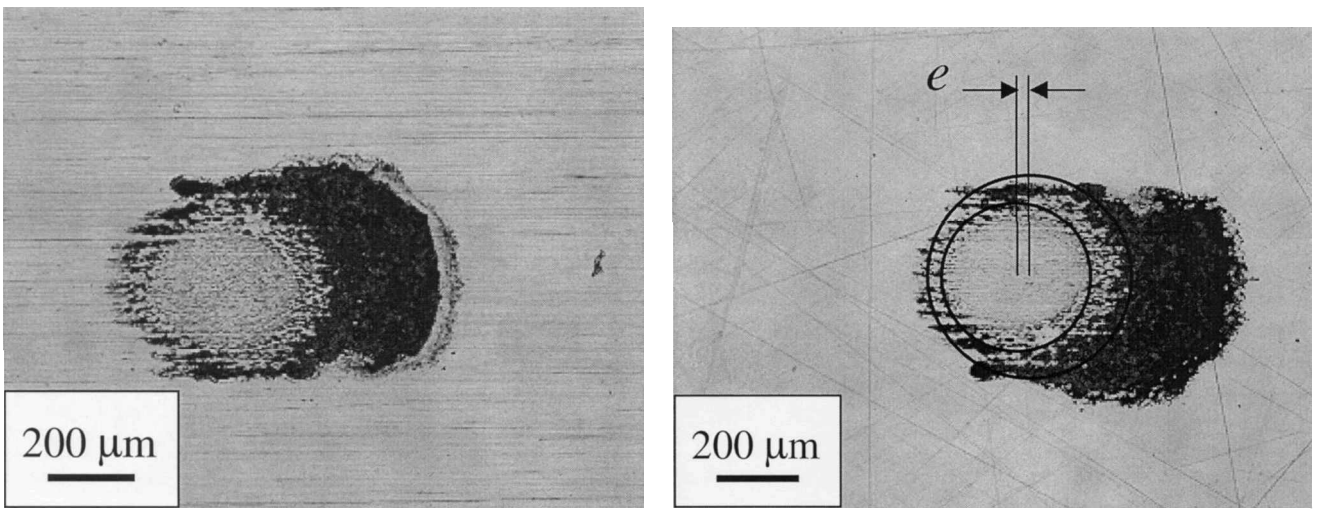

(*a*) (*b*)

Fig. 6—Fretting fatigue scars on (*a*) the fretting pad and (*b*) the sample surface, for an experiment with the normal, tangential, and bulk loads being 50 N, 36 N, and 300 MPa, respectively (the pad radius was 12.7 mm). The circles are obtained theoretically (Eq. 1) and the eccentricity, e (Eq. 3) is fitted to the observed stick zone.

Table IV. List of Experiments Where the Observed Fretting Scar Dimensions (Contact Radius *a*, Stick-Zone Radius *c*, and Eccentricity *e*) Are Compared to Theoretical Predictions (Subscripts *p* and *m* Refer to Predicted and Measured Quantities; and MA and STOA Refer to MA and Solution Treated and Overaged Ti-6Al-4V). For a discussion on eccentricity *e*, see Section IV–A

Test	Material	σ_b	Q (N)	N (N)	R (mm)	a_p (μm)	a_m (μm)	c_p (μm)	c_m (μm)	e_p (μm)	e_m (μm)
1	MA	300	36	50	25.4	244	238	152	179	54.2	31
2	MA	300	36	50	25.4	244	253	152	167	54.2	13.3
3	MA	300	22.5	50	25.4	244	253	197	206	54.2	26.7
4	MA	300	22.5	50	25.4	244	273	197	193	54.2	26.7
5	STOA	300	17	50	12.7	194	200	167	143	27.1	20
6	MA	300	17	50	12.7	194	220	167	200	27.1	23.3
7	STOA	300	19.5	50	12.7	194	185	172	125	27.1	23.8
8	STOA	300	17	50	12.7	194	200	167	133	27.1	66.7
9	MA	300	17	25	25.4	194	200	127	173	54.2	26.7

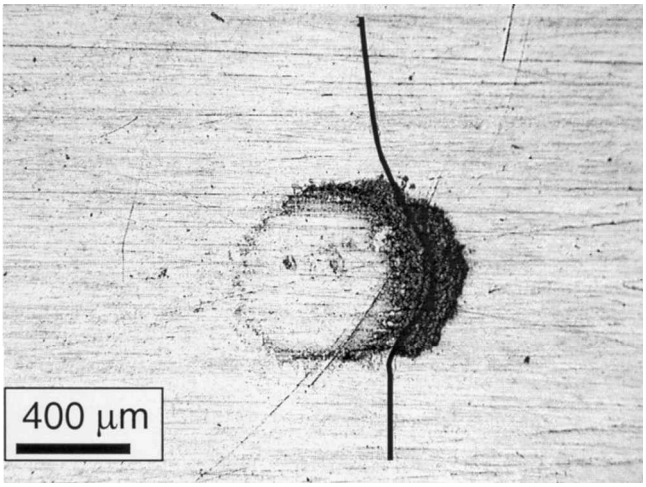

Fig. 7—Fretting fatigue crack observed in the MA Ti-6Al-4V tested under the following conditions: R = 12.7 mm, N = 50 N, Q_{max} = 21 N, and σ_b = 300 MPa; test stopped after 290,000 cycles.

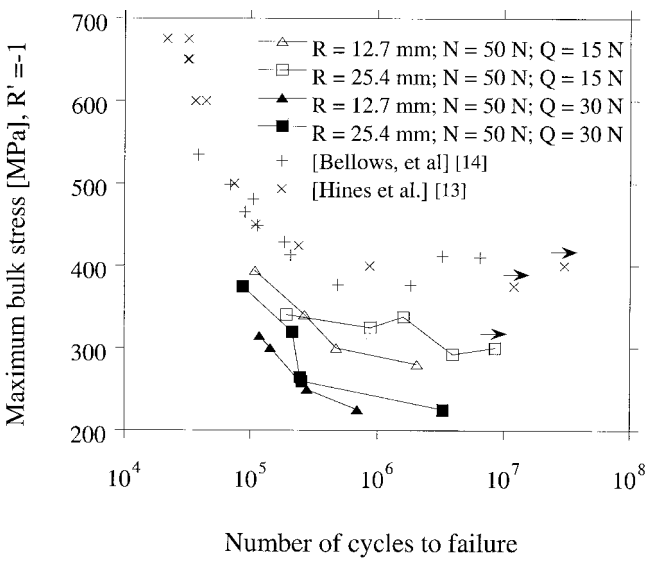

Fig. 8—Fretting fatigue results from experiments on the MA Ti-6Al-4V illustrating variation of total life with changes in the bulk stress applied to the specimen, for a variety of contact geometry and loading conditions. Uniaxial fatique results from ref. [13] and [14].

the bulk stress, and the fretting pad radius were maintained constant while the tangential load was varied by changing the compliance of the system (Figure 9). In general, the total life to failure of the fretted materials was reduced as the tangential load increased, the reduction in life being larger for the experiments with the lower pad radius of 12.7 mm.

D. *Effect of the Normal Load*

Two sets of experiments were conducted on the MA material (tests 29–36, Table III), where for each set, the tangential load, the bulk stress, and the fretting pad radius were maintained constant while the normal load was varied (Figure 10). The total life to failure of the fretted materials increased as the normal load increased, the increase in life being larger for the experiments with the larger pad radius of 25.4 mm.

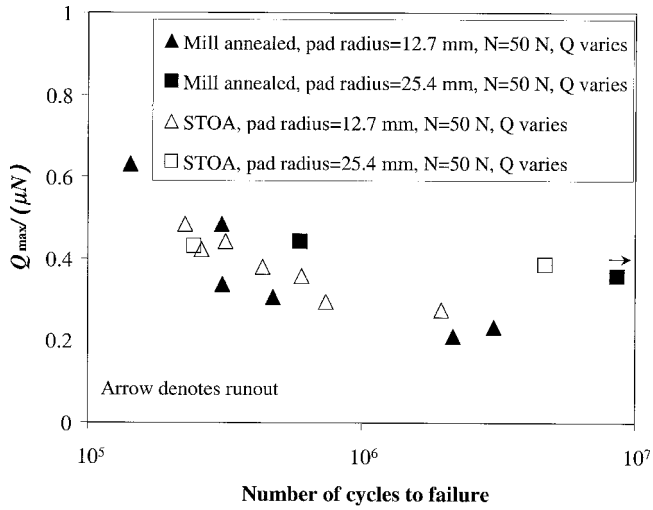

Fig. 9—Fretting fatigue results from experiments on the MA and STOA Ti-6Al-4V illustrating variation of total life with changes in the tangential loads applied to the fretting contact, for a variety of contact geometry (σ_b = 300 MPa, and μ = 0.95).

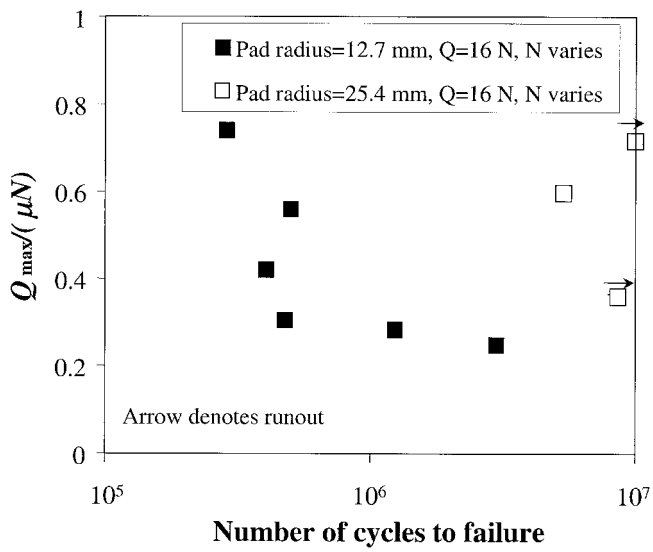

Fig. 10—Fretting fatigue results from experiments on the MA Ti-6Al-4V illustrating variation of total life with changes in the normal loads applied to the fretting contact, for a variety of contact geometry (σ_b = 300 MPa, and μ = 0.95).

E. *Effect of the Microstructure*

One set of experiments was conducted on the materials with different microstructures: martensitic (tests 47 through 52, Table III), coarse STOA (tests 53 and 54, Table III), Widmanstätten (tests 55 and 56, Table III), and acicular (test 57, Table III), where the bulk and the normal loads were maintained constant while the tangential load was varied. With the exception of the martensitic structure, where preliminary results suggested an enhanced fretting fatigue resistance (Figure 11), the other microstructures did not exhibit a significant improvement in fretting fatigue resistance, compared to the basic STOA or the MA microstructure. The martensitic material also exhibited higher Vicker's hardness as compared to other microstructures (Figure 12).

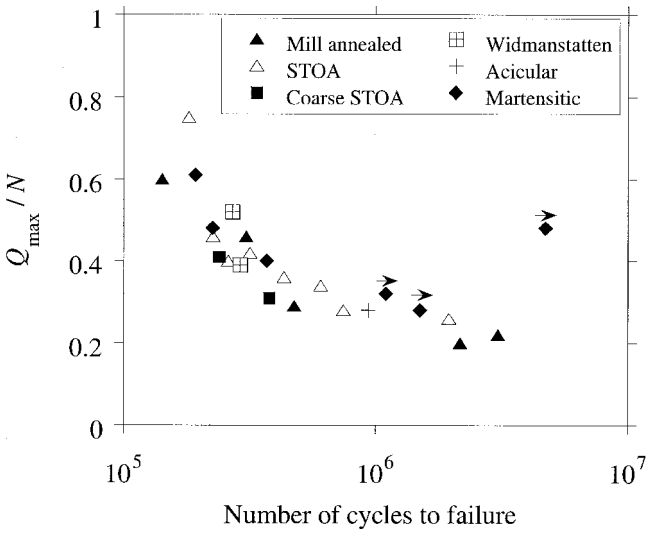

Fig. 11—Fretting fatigue results from experiments on Ti-6Al-4V with different microstructures illustrating variation of total life with changes in the tangential loads applied to the fretting contact (σ_b = 300 MPa, R = 12.7 mm, and N = 50 N).

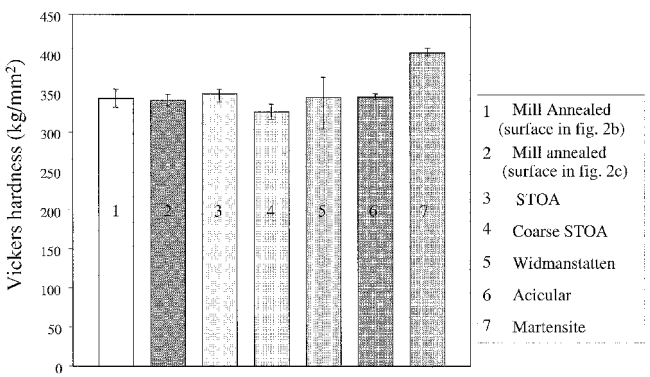

Fig. 12—The average Vickers hardness of different Ti-6Al-4V microstructures.

IV. DISCUSSION

A. *Fretting Scars and Friction*

A sphere of diameter, D, elastic modulus, E, and Poisson ratio, ν, contacting the planar surface of a large substrate of similar material, under an elastic load, N, results in a contact radius, a, given as[15]

$$a = \left[\frac{3D(1-\nu^2)}{4E}N\right]^{1/3} \qquad [1]$$

From Table IV, it is evident that the observed contact radii correlate well with theoretical predictions of Eq. [1].

Upon the application of an oscillatory tangential load, $-Q_{max} \le Q \le Q_{max}$, to the contact *via* the fretting pad, under stick-slip conditions (*i.e.*, $(Q/N) < \mu$, where μ is the coefficient of friction), the radius of the stick zone, c, is given as[16]

$$c = a\left[1 - \frac{Q_{max}}{\mu N}\right]^{1/3} \qquad [2]$$

For the case where the oscillatory tangential load, at the contact interface, is generated through the application of an oscillatory bulk stress, $-\sigma_b \le \sigma \le \sigma_b$, to the substrate, the radius of the stick zone remains unchanged at c. But the center of the stick zone is displaced from the center of the contact area by e, defined as the eccentricity of the contact, given approximately as[8]

$$e \approx \frac{(1-\nu)}{(4-3\nu)}\frac{4\sigma_b a}{\pi\mu p_{max}} = \frac{(1-\nu)(1-\nu^2)}{(4-3\nu)}\frac{2\sigma_b D}{\mu E} \qquad [3]$$

where $p_{max} = \dfrac{3N}{2\pi a^2}$.

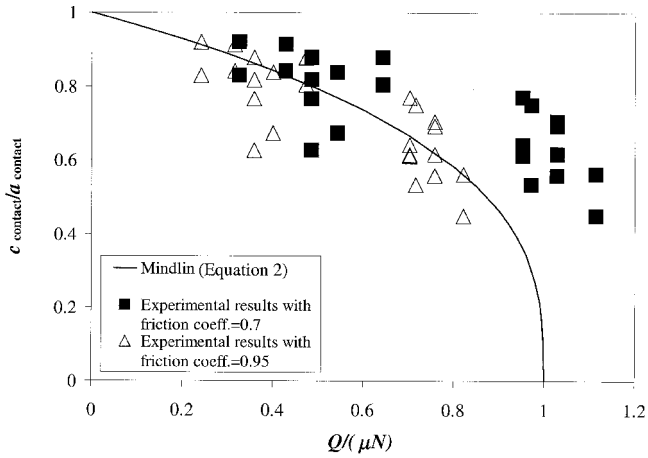

Fig. 13—The experimentally determined fretting scar sizes compared to theoretical predictions for two different values for the coefficient of friction, illustrating a better fit for μ = 0.95.

As seen in Eq. [2] and [3], the theoretical predictions for the stick-zone radius, c, and the eccentricity, e, depend on the friction coefficient. Using the measured maximum static (or breakaway) friction coefficient of 0.95 for Ti-6Al-4V (Appendix A), there is good agreement between the theoretical prediction of Eq. [2] and the experimentally observed values for the stick-zone radius (Table IV). From Figure 13, it is evident that compared to using the sliding friction coefficient of 0.7, the use of the maximum static friction coefficient of 0.95 results in a better match between the experimental observations and predictions from Eqs. [1] and [2] for the contact and stick-zone radii, respectively.

The observed eccentricities compare reasonably well with those predicted by Eq. [3] for experiments with a fretting pad radius of 12.7 mm. However, for those experiments with a fretting pad radius of 25.4 mm, the observed values are a factor of 2 less than the predicted ones. This observation is consistent with the general expectation that for combinations of conditions where the expected eccentrities are low, *i.e.*, low bulk stress and/or pad diameter, or high friction coefficient and/or modulus, Eq. [3] provides good estimates for eccentricities.

B. *Fretting Fatigue Crack Initiation and Propagation*

In general, the fretting fatigue phenomenon can be envisioned as encompassing four regions (Figure 14):

(I) crack initiation,
(II) crack propagation under the combined influence of contact and bulk loads,

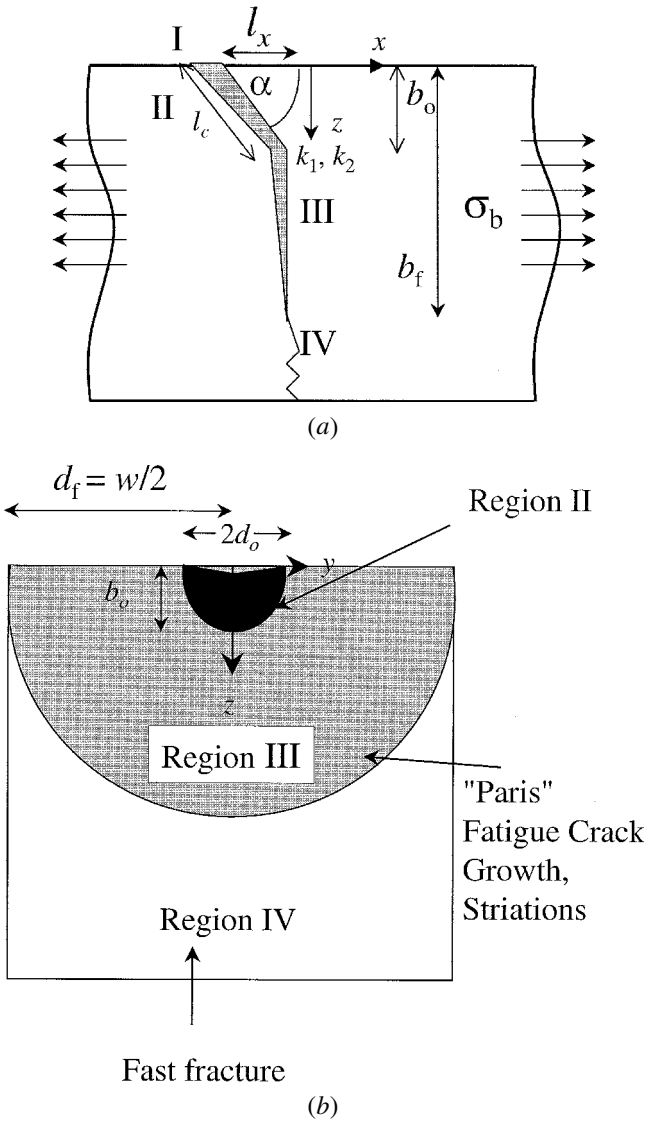

Fig. 14—Schematic illustrating different regions of fretting fatigue cracking in (*a*) the longitudinal section and (*b*) the lateral cross section of the specimen.

(III) crack propagation under the influence of the bulk load only, and
(IV) catastrophic component failure.

I. *Crack initiation*

Traditionally, several criteria such as Crossland, max shear stress, Findley, Sines, Smith-Watson-Topper, McDiarmid, and Papadopoulos (as reviewed in Reference 5), which are based on different combinations of stresses at a critical location in the contact zone, have been invoked to predict crack initiation. These methods are typically applied to loading scenarios where the stresses in the contact zone are finite. It has been recently demonstrated[6] that under conditions where the contacting surfaces adhere to each other, tensile stress singularities could develop, either at the edge of the contact or at the stick-slip boundary, depending on the strength of adhesion. Hence, the direct application of any stress-based criterion to adhesive contact scenarios (where infinite stresses are predicted) would lead to the prediction that cracks initiate regardless of the magnitudes of the

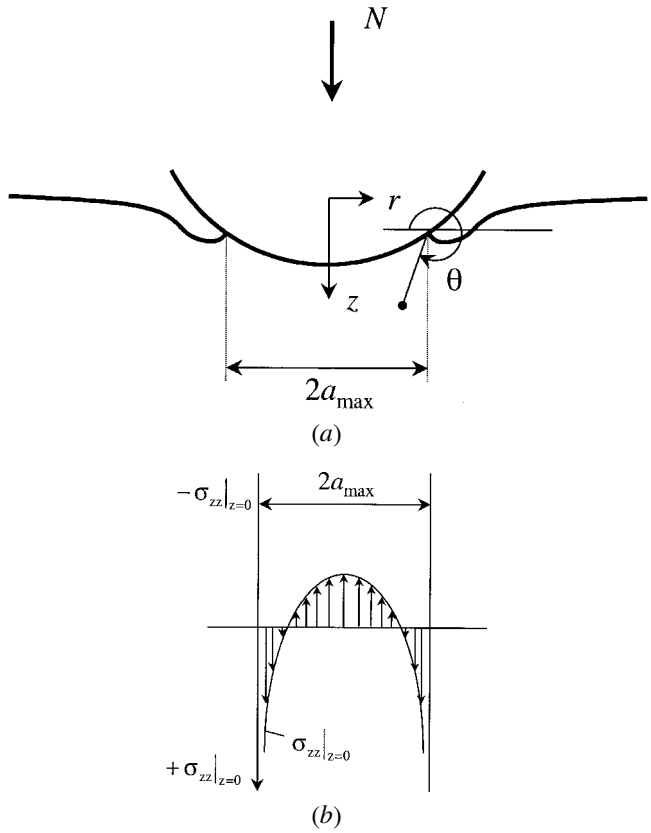

Fig. 15—Schematics illustrating (*a*) adhesive contacts and (*b*) the corresponding stress field exhibiting tensile square-root singularity.[6]

applied contact loads, contrary to experimental observations. Hence, we invoke a fracture mechanics based approach, which provides a framework to deal with such stress singularities.

By noting that the adhesion induces square-root singular stress fields in the asymptotic limit, an analogy can be made between the (real) sphere-on-flat substrate adhesive contact and a (virtual) circumferential cracked body with an uncracked ligament equal to the contact zone (Figure 15). The procedure for deriving the corresponding cyclic stress intensity factors as a function of the work of adhesion, loading, conditions, and geometry, for the case of the contact fatigue scenario, has been described in detail in Reference 6 and is summarized in brief below.

Under adhesive conditions, when two surfaces with surface energies γ_1 and γ_2 adhere to form a new interface of lower energy, γ_{12}, the corresponding work of adhesion is defined as $w' = (\gamma_1 + \gamma_2 - \gamma_{12}) \geq 0$. For two contacting solids with the same elastic properties, which are presently considered, $w' = 2\gamma_1$. For metals, $w' \approx 1$ N/m.[17]

For a sphere of diameter, D, elastic modulus, E, and Poisson ratio, ν, contacting the planar surface of a large substrate of similar material, under an applied normal load N_{max}, the short-range forces of attraction that promote adhesion effectively increase the contact load across the interface and thus increase the contact radius, a_{max} (Figure 15), given as

$$a_{max} = \left[\frac{3D(1-\nu^2)}{4E}\left(N_{max} + \frac{3\pi D w'}{2}\right.\right. \quad [4]$$

$$+ \sqrt{3\pi D w' N_{\max} + \left(\frac{3\pi D w'}{2}\right)^2}\Bigg)\Bigg]^{\frac{1}{3}}$$

and the maximum tangential load, $\overline{Q}_{\max}$, that can sustain adhesion at maximum contact radius is

$$\overline{Q}_{\max} = 2\sqrt{\frac{(2-2\nu)}{(2-\nu)}\pi a_{\max}^3\left[G_d^{\mathrm{II}}\frac{E}{(1-\nu^2)} - \left(\frac{3G_d^{\mathrm{I}}\pi D}{4a_{\max}^{3/2}}\right)^2\right]} \quad [5]$$

where G_d^{I} and G_d^{II} are the critical debonding energies under pure normal and tangential loads, respectively. The debonding energy, G_d (N/m), can be empirically related to the friction coefficient as[6,18]

$$G_d = 14.4\,(0.3 + \mu^2)^{1/2} \quad [6]$$

If the amplitude of the applied tangential load $Q_{\max} \le \overline{Q}_{\max}$, strong adhesion (stick) is obtained.

The stress-intensity factor, K_{I}, that corresponds to the mode I (steady) crack field is given by[6]

$$K_{\mathrm{I}} = \frac{N^*_{\max} - N_{\max}}{2a_{\max}\sqrt{\pi a_{\max}}} \quad [7]$$

where the apparent load, $N^*_{\max}$, required to maintain the same contact radius, $a_{\max}$, without adhesion is given by Hertzian analysis:

$$N^*_{\max} = \frac{4Ea_{\max}^3}{3\,(1-\nu^2)D} \quad [8]$$

The stress-intensity factor that corresponds to mode II (oscillatory) crack fields at the leading and the trailing contact edges is given by

$$\Delta K_{\mathrm{II}} = \frac{Q_{\max}}{a_{\max}\sqrt{\pi a_{\max}}} \quad [9]$$

with the local effective load ratio $R' = -1$.

If the amplitude of the applied tangential load $Q_{\max} \ge \overline{Q}_{\max}$, then weak adhesion (stick slip) is obtained resulting in a partial slip annulus, $c \le r \le a_{\max}$.

From global equilibrium,

$$Q_{\max} = \mu N_{\max}\left[1 - \left(\frac{c}{a_{\max}}\right)^3\right]; \quad \overline{Q}_{\max} < Q_{\max} \le \mu N_{\max} \quad [10]$$

The tangential load that is balanced in the stick zone of radius c is

$$Q^{\mathrm{in}}_{\max} = Q_{\max} - \mu\frac{N_{\max}}{a^3_{max}}(a^2_{\max} - c^2)^{3/2} \quad [11]$$

In this case, $K_{\mathrm{I}} = 0$, as the model predicts a closed crack tip.[6]

The mode II stress intensity factor at the leading and trailing edge of the stick-slip interface is given by

$$\Delta K_{\mathrm{II}} = 2 \times \min\left(\frac{Q^{\mathrm{in}}_{\max}}{2c\sqrt{\pi c}}, \sqrt{\frac{G_d^{\mathrm{II}}E}{1-\nu^2}}\right) \quad [12]$$

with the local load ratio $R' = -1$.

A fatigue crack is expected to initiate at the contact perimeter or the stick-slip boundary, for strong or weak adhesion, respectively, if the corresponding $\Delta K_{\mathrm{II}} \ge \Delta K_{th}$, where ΔK_{th} is the threshold stress intensity range that corresponds to $R' = -1$, and under mixed constant mode I and oscillatory mode II fatigue. This situation holds both for strong adhesion and under pure oscillatory mode II fatigue for weak adhesion.

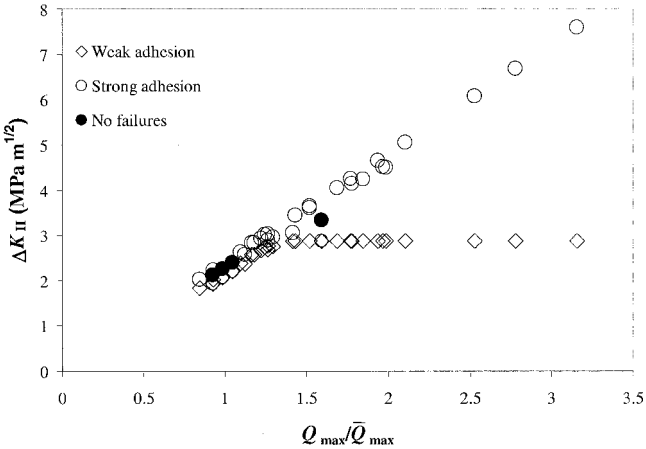

Fig. 16—Room-temperature fretting fatigue experiments on Ti-6Al-4V evaluated using the adhesion model, where the mode II threshold stress-intensity factor for an R' ratio of -1 was estimated to be ≈ 2 MPa$\sqrt{\text{m}}$ and the work of adhesion for advancing and receding contacts (w, G_d) to be ≈ 1 and ≈ 15.8 N/m, respectively.

The fretting fatigue experiments on Ti-6Al-4V can be analyzed within the context of the adhesion model, using the material parameters (Table II), threshold $\Delta K_{\mathrm{II}} \approx 2$ MPa$\sqrt{\text{m}}$ (estimated from[19]), and the experimentally determined friction coefficient, $\mu = 0.95$. Using reasonable values for the work of adhesion for advancing and receding contacts, $w' = 1$ N/m and $G_d = 15.8$ N/m (Eq. [6]), the adhesion model predicts weak adhesion, in agreement with experiments where in all cases stick-slip behavior was observed (Figure 16).

However, while the model predicts cracks to initiate at the stick-slip boundary, in many cases, the cracks were found to have initiated in the slip zone and sometimes closer to the edge of the contact. This might indicate that conditions of strong adhesion may have existed prior to the development of the partial slip during which time the cracks could have initiated at the edge of the contact.

II. *Crack propagation under the combined influence contact and bulk loads*

Upon initiation, the continued propagation of the crack tip depends on the local mode I and mode II stress intensity factors, k_1 and k_2, respectively (Figure 14). Following Cottrell and Rice,[20] it is postulated that the crack advances in a direction along which the local mode II stress intensity factor k_2 vanishes. The initial angle of crack propagation, α, is then obtained from

$$k_2 = \frac{1}{4}\left(\sin\frac{\alpha}{2} + \sin\frac{3\alpha}{2}\right)K_{\mathrm{I}} + \frac{1}{4}\left(\cos\frac{\alpha}{2} + 3\cos\frac{3\alpha}{2}\right)K_{\mathrm{II}} = 0 \quad [13]$$

While the model predicts an initial crack angle of 70.5 deg, the observed crack initiation angles (computed as $\alpha = \arctan(b_0/l_x)$, where b_0 and l_x are as illustrated in Figures

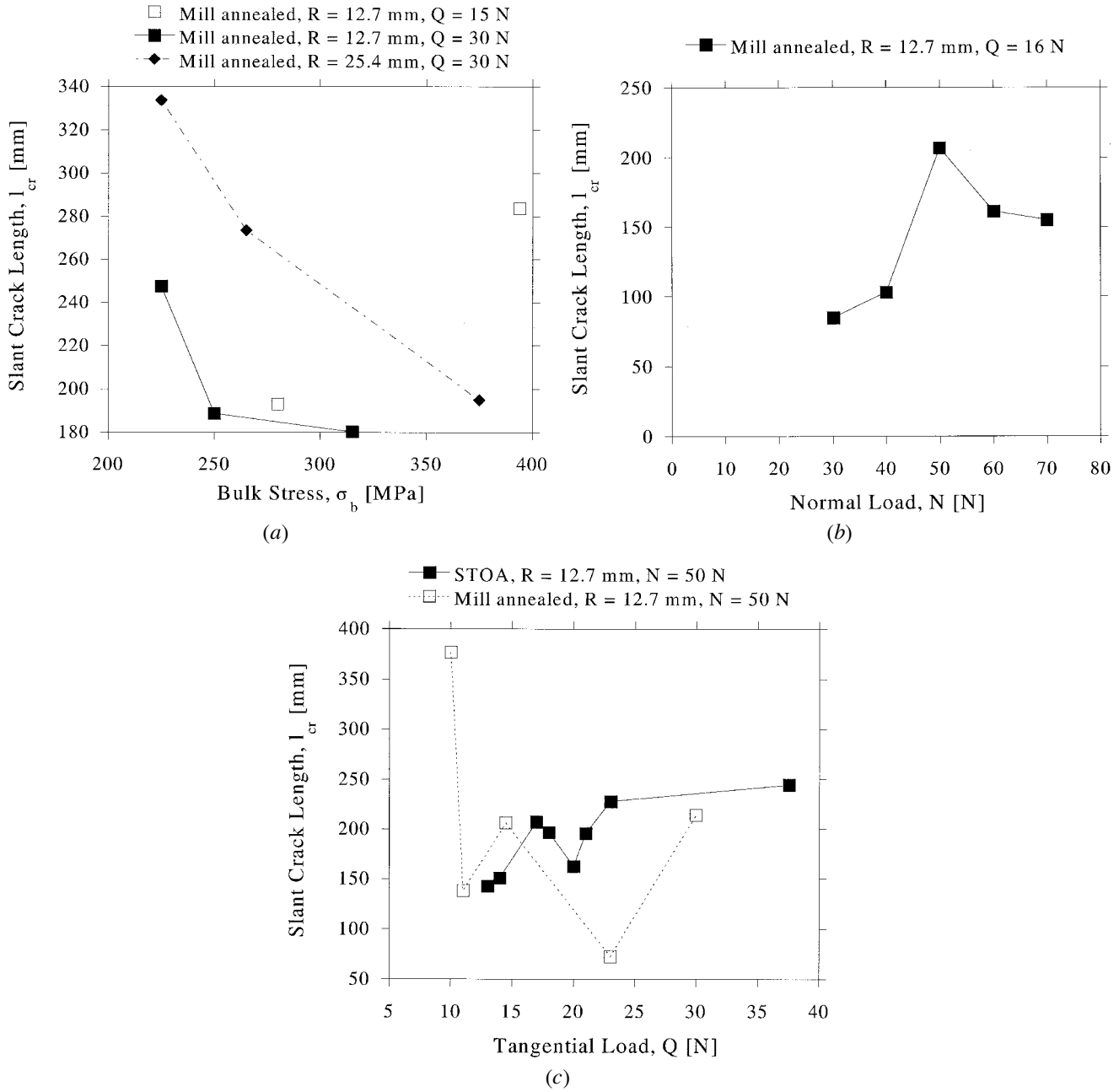

Fig. 17—The effects of the (*a*) bulk stress, (*b*) the normal load, and (*c*) the tangential load on the slant crack length.

14(b) and Ca), had a mean of 68 deg with a standard deviation of 8 deg (Table III).

As the small surface crack grows further into the substrate, the effects of the contact loads, N, and ΔQ, in providing a sufficiently large Δk_1 to advance the crack tip, rapidly diminish, leading to a competition between the applied uniform cyclic bulk stress, $\Delta\sigma_b$ and the contact loads. After some initial growth over a distance l_c into the substrate, the crack is expected to reorient itself normal to the applied tensile cyclic stress $\Delta\sigma_b$. If at the critical distance l_c, the tensile opening stress intensity factor due to the applied loads is larger than the effective mode I threshold stress intensity factor range, ΔK_{th}, the crack would reorient itself normal to the uniform applied stress and would continue to advance into the substrate in mode I. Otherwise, the crack is expected to arrest completely.

From an inspection of results from tests 13, 15, and 16 as well as 17, 19, and 21 (Table III), it is apparent that with an increase in the bulk stress (while the contact loads and fretting pad radius were maintained constant), the critical slant crack length, l_c, decreases, as expected (Figure 17(a)). An exception to the general trend is noted in tests 1 and 5, where l_c is found to be higher in test 1 compared to test 5.

From tests 29 through 34 (Table III), it is evident that at higher normal loads (>50 N), an increase in the normal loads (while the bulk stress and the tangential loads are maintained constant) results in a decrease in the critical slant

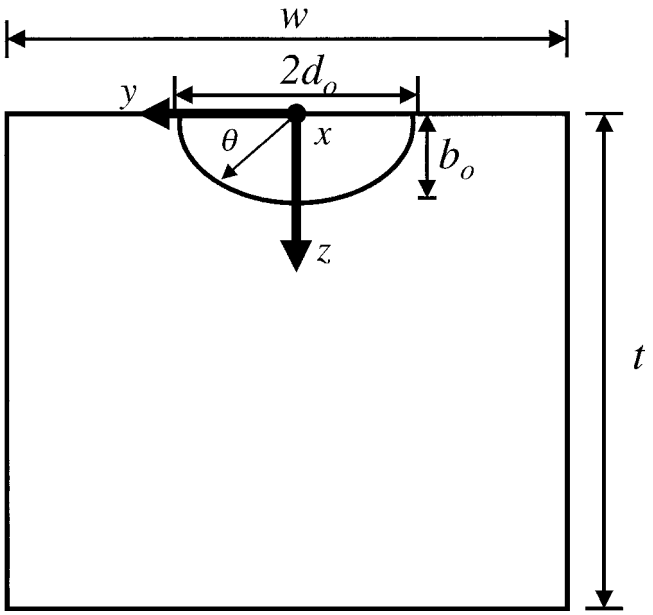

Fig. 18—Schematic illustrating the various input geometric parameters for the calculation of the stress-intensity factors for the fretting fatigue crack in region III.

crack length, l_c (Figure 17(b)). This observation is consistent with the expectation that an increase in the normal loads would tend to decrease the mode I stress intensity factor at the tip of the slant crack, Δk_I, thus reducing l_c. In the limiting case, where the normal loads tend to zero, the contact fields are expected to be very weak and fatigue cracking is expected to be dominated by the bulk stress. Consequently, the slant crack lengths are expected to be small, thus explaining the smaller slant crack lengths observed at lower normal loads (<50 N).

It is expected that an increase in the tangential loads would tend to promote slant crack growth in region II and thus increase l_c. This general trend in observed in tests 37 through 44 (Table III), while considerable scatter exists in the results of tests 22 through 26 (Table III, Figure 17(c)).

III. *Crack propagation under the influence of bulk load only*

An inspection of the fractured surfaces of the specimens indicates that the crack shape at the end of region II could be approximated as being semielliptical (Figure 18). The subsequent propagation of the crack in region III, under the influence of the bulk loads, $\Delta\sigma_b$, in a plane perpendicular to the applied bulk load, can be modeled as being driven by the crack-tip stress intensity factor:[21]

$$K_I = \sigma_b \sqrt{\frac{\pi b}{Q'}} \times F\left(\frac{b}{t}, \frac{b}{c}, \frac{d}{w}, \theta\right) \qquad [14]$$

where

$$Q' = 1 + 1.464\left(\frac{b}{d}\right)^{1.65},$$

$$F = \left[M_1 + M_2\left(\frac{b}{t}\right)^2 + M_3\left(\frac{b}{t}\right)^4\right] f_\theta g f_w$$

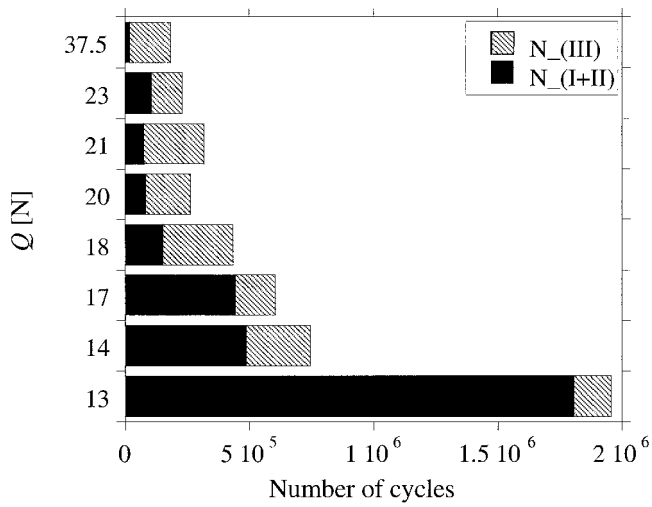

Fig. 19—Analysis of fretting experiments (37 through 44, Table III), illustrating fretting life in the different regions. (In all these cases, $N = 50$ N, $R = 12.7$ mm, and $\sigma_b = 300$ MPa).

$$M_1 = 1.13 - 0.09\left(\frac{b}{d}\right), \quad M_2 = -0.54 + \frac{0.89}{0.2 + b/d},$$

$$M_3 = 0.5 - \frac{1.0}{0.65 + b/d} + 14\left(1.0 - \frac{b}{d}\right)^{24} \qquad [15]$$

$$g = 1 + \left[0.1 + 0.35\left(\frac{b}{t}\right)^2\right](1 - \sin\theta)^2,$$

$$f_\theta = \left[\left(\frac{b}{d}\right)^2 \cos^2\theta + \sin^2\theta\right]^{1/4}$$

$$f_w = \left[\sec\left(\frac{\pi d}{2w}\sqrt{\frac{b}{t}}\right)\right]^{1/2}$$

The rate of crack propagation, in region III, is taken as following a Paris-type power law:

$$\frac{db}{dN} = C\,(\Delta K_I)^m \qquad [16]$$

where C and m are material constants. For mill-annealed Ti-6Al-4V, C and m were determined from low load ratio experiments (accounting for crack closure), respectively, as 7.5×10^{-13} and 4.1 (where db/dN_{III} and ΔK_I were in the units of m/cycle and MPa$\sqrt{\text{m}}$, respectively).[22]

The mode I stress intensity factor range, ΔK_I, is given as $\Delta K_I = (1 - R')K_{max}$, where K_{max} is the stress intensity factor that corresponds to monotonic loading. For fully reversed fatigue loading with $R' = -1$, $\Delta K_I = 2K_I$. The life of the specimen in region III can be obtained through the integration of the Paris law (Eq. [16]) between the limits (b_0, d_0) and (b_f, d_f), where $d_f = (w/2)$. Assuming the specimen fractures catastrophically in the final cycle, the total life spent by the specimen in the several regions is presented in Table III.

As illustrated in Figure 19, for experiments where the bulk stress and the normal contact loads were maintained constant, the life spent in regions I and II scales with the tangential load, while the life spent in region III remains almost constant, as expected. From an inspection of results

from tests 1 and 5, 13, 15, and 16 as well as 17, 19, and 21 (Table III), it is apparent that with an increase in the bulk stress (while the contact loads and fretting pad radius were maintained constant), the fraction of fretting fatigue life spent by the specimen in the third region, N_{III}, decreases, as expected.

IV. *Catastrophic component failure*

While the mode I fracture toughness, K_{IC}, of Ti-6Al-4V can range between 33 and 110 MPa$\sqrt{m}$ depending on the oxygen content and the heat treatment, the mill-annealed and STOA microstructures studied in this work exhibit a fracture toughness of 65 MPa$\sqrt{m}$.[23] As the critical crack length, b_c, that corresponds to this K_{IC} is between 7 and 22 mm, which is much greater than the sample size (5 mm), the sample failure was attributed to mechanical overload.

F. *Effect of Contact Conditions and Microstructure—Overall Analysis*

The observed trends in the variation of the fretting fatigue lives for the different sets of controlled experiments could be examined within the framework presented in Sections IV–A through D (Table V).

(1) An increase in the bulk load (while keeping all other parameters constant) effectively reduces the critical slant crack length, l_c, and thus reduces the life spent in region II. Additionaly, the life in stage III is reduced as well, resulting in a decrease in the total fretting fatigue life.
(2) An increase in the tangential load, Q, increases the effective cyclic mode I stress intensity factor, Δk_1, ahead of the slant crack and thus reduces the life spent in region II. Assuming the life in region III to remain unchanged with changes in Q (to a first order), this analysis predicts the total fretting fatigue life to decrease with an increase in Q.
(3) An increase in the normal load, N, increases the maximum contact pressure, p_{max}. Consequently, Δk_1 decreases as the slant crack tip is effectively shielded. Thus, the life spent in region II increases. Assuming, the life in region III to be invariant with changes in N, the total fretting fatigue life is expected to increase with an increase in N.
(4) An increase in the fretting pad radius, R, decreases the maximum contact pressure and leads to the prediction that the total fretting fatigue life should decrease. However, the experiments indicate that the total fretting fatigue life actually increases with an increase in R. This increase in total life may be attributed to an increase in the life spent in region I (*i.e.*, the crack initiation stage) that is not accounted for in this analysis.
(5) The preliminary study of the effect of microstructure on fretting fatigue in Ti-6Al-4V indicated that the martensitic microstructure might have enhanced fretting resistance. It is possible that this enhanced fretting resistance may be related to the higher yield strength and hardness observed in the martensitic microstructure (Figure 12). The effect of the different microstructures on the crack growth rates in regions II and III needs to be assessed and further work is planned.

V. CONCLUSIONS

From a systematic experimental study of the fretting fatigue response of the titanium alloy Ti-6Al-4V, the following conclusions are drawn.

1. In the experiments where the contact loads were maintained constant while the bulk stress was varied, fretting reduced the fatigue strength of Ti-6Al-4V. Because the slant crack propagation rates in region II are directly and strongly correlated to the tangential load, the strength reduction factor was higher for those experiments with a constant but higher tangential load compared to those with a constant but lower tangential load.
2. For cases where the bulk stress and the normal loads were maintained constant, the total life to failure of the fretted materials was reduced as the tangential load increased. This is consistent with the expectation that higher tangential loads promote faster fretting fatigue crack growth in region II.
3. In the experiments where the bulk stress and the tangential loads were maintained constant, the total life to failure of the fretted materials increased as the normal load increased. This was due to the fact that higher normal loads tend to reduce the slant crack propagation rate in region II.
4. In general, the increase in pad radius tended to increase

Table V. An Overall Summary of the Comparison between the Predicted Trends and the Experimental Observations for the Different Sets of Fretting Experiments (with a Load Ratio $R' = -1$) Where the Test Parameters Such as the Bulk Stress (σ_b), the Tangential Load (Q), the Normal Load (N), and the Pad Radius (R) Were Varied Systematically

					a		c		c/a						N_f	
σ_b	Q	N	R	p_{max}	Predicted	Observed	Predicted	Observed	Predicted	Observed	Δk_I	$N_{(I+II)}$	$N_{(III)}$	Predicted	Observed
Increases	Constant	Constant	Constant	Constant	Constant	Constant	Constant	Constant	Constant	Constant	Constant	Decreases	Decreases	Decreases	Decreases
Constant	Increases	Constant	Constant	Constant	Constant	Constant	Decreases	Decreases	Decreases	Decreases	Increases	Decreases	Constant	Decreases	Decreases
Constant	Constant	Increases	Constant	Increases	Increases	Increases	Increases	Increases	Increases	Increases	Decreases	Increases	Constant	Increases	Increases
Constant	Constant	Constant	Increases	Decreases	Increases	Increases	Increases	Increases	Constant	Constant	—	—	Constant	—	Increases

Key: Predictions for the different output parameters were obtained as follows.
a = contact radius, Eq. [1].
c = stick-zone radius, Eq. [2].
N_{III} = number of cycles spent in region III, Section IV–C.
N_{I+II} = number of cycles spent in region I + II.
N_I = total fretting fatigue life.
p_{max} = Maximum contact pressure.
Δk_I = cyclic mode I stress intensity factor at the tip of the slant crack in region II.

the total fretting fatigue life. This effect can be attributed to an increase in the crack initiation life (region I).

5. Limited results for the martensitic structure, which had a higher yield stress and hardness compared to the other Ti-6Al-4V microstructures, suggest an enhanced fretting fatigue resistance. However, a more comprehensive study is required to fully assess the fretting response of the martensitic structure.
6. Using the measured maximum static friction coefficient of 0.95 for Ti-6Al-4V, the experimentally observed contact and stick-zone radii exhibited good agreement with analytical predictions.
7. The adhesion model predictions concerning strength of adhesion (*i.e.*, weak adhesion) and conditions for crack initiation and initial crack propagation angles were validated with experimental observations.

ACKNOWLEDGMENTS

This work was supported by the Multi-University Research Initiative on "High Cycle Fatigue," which is funded at MIT by the Air Force Office of Scientific Research, Grant No. F49620-96-1-0478, through a subcontract from the University of California at Berkeley. Assistance from Laurent Chambon with some of the fretting experiments is gratefully acknowledged.

APPENDIX A

Given the important role that friction plays in the fretting fatigue problem, the following experiment was designed to evaluate the average friction coefficient.

At a constant normal contact load (of 10 or 14 or 15 N), conditions of stick slip were first established at a tangential load of 1.0 N, by suitable choice of the bulk stress, at a test frequency, initially at 1 Hz and finally at 10 Hz. The tangential load was then increased (by increasing the bulk stress) until full sliding occurred. The transition from stick slip to full sliding was recognized by following the change in the hysteresis behavior of tangential load with bulk stress, from a closed loop (during stick slip) to an open loop (during full sliding). The ratio of the tangential load to the normal load at this transition is taken as the breakaway (or maximum static) coefficient of friction, $\mu_b = Q/N$.

Immediately following this breakaway, the maximum tangential load decreased to a new steady state, Q_{slip}, and the corresponding dynamic coefficient of friction, μ_d, was taken as $\mu_d = (Q_{slip}/N)$.

After a few thousand cycles of full sliding behavior, conditions of stick slip were re-established, possibly due to an increase in the friction at the contact interface caused by roughening and oxide debris buildup. By increasing the bulk stress, full sliding could be established, albeit at tangential loads greater than that corresponding to the first breakaway point (Figure A1).

For specimens with well-developed fretting scars, the measured breakaway and dynamic friction coefficients, 0.95 and 0.70, respectively, which were independent of the normal contact loads, were slightly larger than those reported in the literature ($\mu_b = 0.85$,[24] $\mu_d = 0.70$,[24] or 0.60[23]).

The upper limit on the maximum static friction coefficient can be estimated by setting max $(G_d) = G_c = (K_{IC}^2/E)$ and

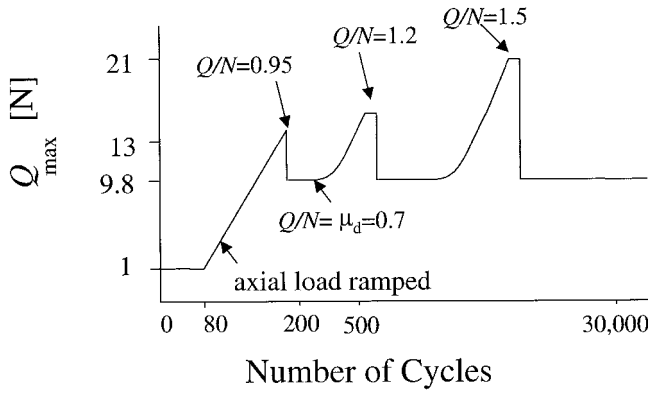

Fig. A1—Schematic illustrating the variation with the number of fatigue cycles of the tangential load as the bulk load on the specimen is increased, indicating onset of full sliding at several values of the tangential loads (under a constant normal load of 14 N).

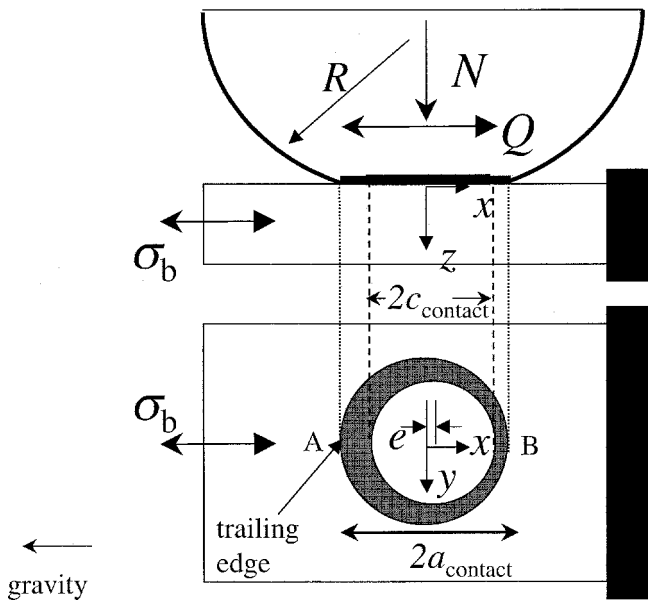

Fig. B1—Schematic illustrating the location of the trailing edge of the contact.

using $K_{IC} = 65$ MPa$\sqrt{\text{m}}$ for Ti-6Al-4V in Eq. [6] to yield max $(\mu) = 2.55$.

It is believed that the maximum static friction coefficient measured in the fretting tests may depend on the velocity of slip (*i.e*, the test frequency) across the contacting interfaces. Hence, in order to be consistent with the fretting experiments (Table III), where the frequency was 10 Hz, the friction measurements were conducted at a test frequency of 10 Hz as well.

APPENDIX B

During one-half of the fatigue cycle, when the sample is fully loaded in tension, the maximum tensile stress created by the tangential loading occurs at location A in the sample. Upon load reversal, the maximum tensile stress due to the tangential load occurs at location B. However, since the sample is under compression, the effective tensile stress at B is much smaller than at A. Thus, location A, which is the

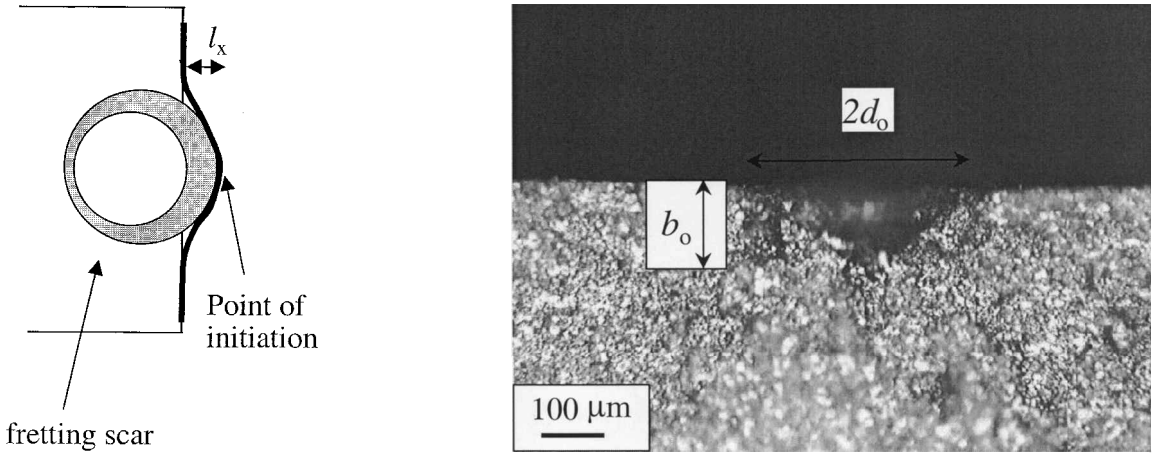

(*a*) (*b*)

Fig. C1—(*a*) Schematic illustrating the location of crack initiation and geometric parameter, l_x. (*b*) Fractured surface indicating the parameter, b_0.

perimeter of the contact closest to the actuator, is designated as the trailing edge of the contact (Figure B1).

APPENDIX C

For the samples that failed, the average angle at which the fretting fatigue cracks initiated in the substrate is obtained through an inspection of two different sections of the specimens, as illustrated in Figure C1. The geometry of the crack as seen from the surfaces gives $\alpha = \arctan(b_0/l_x)$.

REFERENCES

1. R.B. Waterhouse: *Fretting Fatigue*, Applied Science Publishers, London, 1981.
2. R.B. Waterhouse and T.C. Lindley: *Fretting Fatigue*, European Structural Integrity Society Publication 18, London, 1994.
3. R.B. Waterhouse: *Int. Mater. Rev.*, 1992, vol. 37, pp. 77-97.
4. T.C. Lindley: *Int. J. Fatigue*, 1997, vol. 19, pp. S39-S49.
5. I.V. Papadopoulos, P. Davoli, C. Gorla, M. Filippini, and A. Bernasconi: *Int. J. Fatigue*, 1997, vol. 19, pp. 219-35.
6. A.E. Giannakopoulos, T.A. Venkatesh, T.C. Lindley, and S. Suresh: *Acta Mater.*, 1999, vol. 47, pp. 4653-64.
7. B.U. Wittkowsky, P.R. Birch, J. Dominguez, and S. Suresh: *Fatigue Fracture Eng. Mater. Structures*, 1999, vol. 22, pp. 307-20.
8. B.U. Wittkowsky, P.R. Birch, J. Dominguez, and S. Suresh: in *Fretting Fatigue: Current Technology and Practices*, ASTM STP 1367, D.W. Hoeppner, V. Chandrasekaran, and C.B. Elliot, eds., ASTM, Philadelphia, PA, 1999, pp. 213-27.
9. A.L. Hutson, T. Nicholas, and R. Goodman: *Int. J. Fatigue*, 1999, vol. 21, pp. 663-69.
10. R. Cortez, S. Mall, and J.R. Calcaterra: *Int. J. Fatigue*, 1999, vol. 21, pp. 709-17.
11. S. Goto and R.B. Waterhouse: in *Titanium '80: Science and Technology*, H. Kimura and O. Izumi, eds., TMS, Warrendale, PA, 1980, vol. 3, pp. 1837-44.
12. P. Blanchard, C. Colombie, V. Pellerin, S. Fayeulle, and L. Vincent: *Metall. Trans. A*, 1991, vol. 22A, pp. 1535-44.
13. J.A. Hines and G. Lutjering: *Fatigue Fract. Eng. Mater. Structures*, 1999, vol. 22, pp. 657-665.
14. R.S. Bellows, S. Muju, and T. Nicholas: *Int. J. Fatigue*, 1999, vol. 21, pp. 687-697.
15. H. Hertz: *J. Reine. Angewandte Mathematik*, 1882, vol. 92, pp. 156-71.
16. R.D. Mindlin: *J. Appl. Mech.*, 1949, vol. 16, pp. 259-68.
17. V.K. Semenchenko: *Surface Phenomena in Metals and Alloys*, Addison-Wesley, Reading, MA, 1962.
18. J.S. McFarlane and D. Tabor: *Proc. R. Soc., London*, 1950, vol. A202, pp. 244-53.
19. R.O. Ritchie, B.L. Boyce, J.P. Campbell, O. Roder, A.W. Thompson, and W.W. Milligan: *Int. J. Fatigue*, 1999, vol. 21, pp. 653-62.
20. B. Cottrell and J.R. Rice: *Int. J. Fracture*, 1980, vol. 16, pp. 155-69.
21. J.C. Newman and I.S. Raju: *Eng. Fracture Mech.*, 1981, vol. 15, pp. 185-92.
22. G.R. Yoder, L.A. Cooley, and T.W. Crooker: in *Fracture Mechanics: 16th Symp.*, ASTM STP 868, M.F. Kanninen and A.T. Hopper, eds., ASTM, Philadelphia, PA, pp. 392-405.
23. G. Welsch, R. Boyer, and E.W. Collings: *Materials Properties Handbook: Titanium Alloys*, ASM International, Materials Park, OH, 1995.
24. R.A. Antoniou and T.C. Radtke: *Mater. Sci. Eng. A*, 1997, vol. 237, p. 229.